

# Exclusive meson production at HERMES

**Sergey Manaenkov<sup>\*†</sup>**

*NRC “Kurchatov Institute”, Petersburg Nuclear Physics Institute,  
on behalf of the HERMES collaboration*

*E-mail: sman@mail.desy.de*

The data were accumulated with the HERMES forward spectrometer using the 27.6 GeV longitudinally polarized electron or positron beam of HERA. Exclusive electroproduction of  $\omega$  mesons on unpolarized hydrogen and deuterium targets is studied in the kinematic region of  $Q^2 > 1.0 \text{ GeV}^2$ ,  $3.0 \text{ GeV} < W < 6.3 \text{ GeV}$ , and  $-t' < 0.2 \text{ GeV}^2$ , while for  $\rho^0$ -meson production on a transversely polarized hydrogen target  $-t' < 0.4 \text{ GeV}^2$  is used. Spin-density matrix elements for  $\omega$  production are presented in projections of  $Q^2$  or  $-t'$ , while the ratios of the helicity amplitudes for the reaction  $\gamma^* + p \rightarrow \rho^0 + p$  are obtained in the entire kinematic region. The usage of the transversely polarized target allows for the first time the extraction of the ratios of certain nucleon-helicity-flip amplitudes to the natural-parity exchange amplitude  $T_{0\frac{1}{2}0\frac{1}{2}}$  without the nucleon-helicity flip describing the longitudinal  $\rho^0$ -meson production by the longitudinal virtual photon. Violation of  $s$ -channel helicity conservation is observed for both mesons. A dominant contribution from unnatural-parity exchange (UPE) is established for special combinations of the  $\omega$  spin-density matrix elements. For  $\rho^0$ -meson production, the UPE amplitude without the nucleon-helicity flip,  $U_{1\frac{1}{2}1\frac{1}{2}}$ , is shown to be the largest UPE amplitude. Good agreement is found between the HERMES data on  $\omega$  production on the proton and results of the perturbative QCD-inspired Goloskokov-Kroll model that includes pion-pole contribution.

*XXIV International Workshop on Deep-Inelastic Scattering and Related Subjects  
11-15 April, 2016  
DESY Hamburg, Germany*

<sup>\*</sup>Speaker.

<sup>†</sup>Thanks to the Organizing Committee for the invitation to DIS16

## 1. Introduction

Exclusive electroproduction of vector mesons ( $V$ ) on nucleons ( $N$ ) gives information both on the reaction mechanisms and the nucleon structure [1]. Electroproduction at high energies can be considered to consist of three subprocesses: i) the incident lepton emits a virtual photon  $\gamma^*$ , which dissociates into a quark-antiquark pair; ii) this  $q\bar{q}$  pair interacts strongly with the nucleon; iii) the observed vector meson is formed from the scattered  $q\bar{q}$  pair. In Regge phenomenology, the interaction of the  $q\bar{q}$  pair with the nucleon proceeds through the exchanges of a pomeron or/and exchanges of secondary reggeons. If the quantum numbers of the particle lying on the Regge trajectory are  $J^P = 0^+, 1^-, \text{etc.}$  (pomeron,  $\rho, f_2, \dots$ ), the process is denoted Natural Parity Exchange (NPE). Alternatively, the case of  $J^P = 0^-, 1^+, \text{etc.}$  ( $\pi, a_1, \dots$ ) corresponds to Unnatural Parity Exchange (UPE). In the framework of perturbative quantum chromodynamics valid at large photon virtuality  $Q^2$  and high photon-nucleon center-of-mass (CM) energy  $W$ , the nucleon structure can also be studied through hard exclusive meson production, as the process amplitude contains Generalized Parton Distributions (GPDs) (see review [1]). However, the factorization property that permits to extract GPDs is rigorously proved in Ref. [2] only for the amplitude  $F_{00}$  of longitudinal vector meson production by longitudinal virtual photons. In the Goloskokov-Kroll (GK) model (see [3] and references therein), the validity of factorization is assumed for some other amplitudes in addition to  $F_{00}$  and this assumption is justified with a good description of the existing data.

Recently, Spin-Density Matrix Elements (SDMEs) were studied by CLAS [4] for exclusive  $\omega$  electroproduction at  $1.6 \text{ GeV}^2 < Q^2 < 5.2 \text{ GeV}^2$  and the contribution of the  $\pi$ -reggeon was found to be dominant even for large  $Q^2$ . The presented HERMES data [5] can also be well described in the GK model if the pion exchange is taken into account. This means that the GPD-based approach should be modified at intermediate energies and  $Q^2$ .

All observables in vector-meson electroproduction can be expressed in terms of the helicity amplitudes in the CM system of the process  $\gamma^* + N \rightarrow V + N$ , in particular, SDMEs are functions of the helicity amplitude ratios (HARs). Therefore HARs can be extracted from the data as was shown in Ref. [6]. For the first time, HARs with nucleon-helicity flip are obtained in the present analysis from the data on  $\rho^0$ -meson production on a transversely polarized hydrogen target.

## 2. Helicity Amplitudes

The angular distribution of the final-state particles depends on the SDMEs. In the present paper, the formalism proposed in Ref. [7] for SDMEs  $r_{\lambda_V \lambda'_V}^\alpha$  is used. The SDMEs can be expressed in terms of the helicity amplitudes  $F_{\lambda_V \lambda'_N \lambda_\gamma \lambda_N}$  of the process  $\gamma^*(\lambda_\gamma) + N(\lambda_N) \rightarrow V(\lambda_V) + N(\lambda'_N)$ , where the particle helicities are given in parentheses. The helicity amplitudes depend on  $W$ ,  $Q^2$ , and  $t' = t - t_{\min}$ , where  $t$  is the Mandelstam variable and  $-t_{\min}$  represents the smallest kinematically allowed value of  $-t$  at fixed  $W$  and  $Q^2$ .

Any helicity amplitude can be decomposed into a sum of a NPE ( $T_{\lambda_V \lambda'_N \lambda_\gamma \lambda_N}$ ) and an UPE ( $U_{\lambda_V \lambda'_N \lambda_\gamma \lambda_N}$ ) amplitude:  $F_{\lambda_V \lambda'_N \lambda_\gamma \lambda_N} = T_{\lambda_V \lambda'_N \lambda_\gamma \lambda_N} + U_{\lambda_V \lambda'_N \lambda_\gamma \lambda_N}$ , for details see Refs. [7, 8]. The amplitudes obey the symmetry relations that hold because of parity conservation (see, e.g., Ref. [7])

$$T_{\lambda_V \lambda'_N \lambda_\gamma \lambda_N} = (-1)^{-\lambda_V + \lambda_\gamma} T_{-\lambda_V \lambda'_N -\lambda_\gamma \lambda_N} = (-1)^{-\lambda_N + \lambda'_N} T_{\lambda_V -\lambda'_N \lambda_\gamma -\lambda_N}, \quad (2.1)$$

$$U_{\lambda_V \lambda'_N \lambda_\gamma \lambda_N} = -(-1)^{-\lambda_V + \lambda_\gamma} U_{-\lambda_V \lambda'_N -\lambda_\gamma \lambda_N} = -(-1)^{-\lambda_N + \lambda'_N} U_{\lambda_V -\lambda'_N \lambda_\gamma -\lambda_N}. \quad (2.2)$$

These symmetry properties of the helicity amplitudes permit to introduce the abbreviated notations:

$$T_{\lambda_V \lambda_\gamma}^{(1)} \equiv T_{\lambda_V \frac{1}{2} \lambda_\gamma \frac{1}{2}}, \quad U_{\lambda_V \lambda_\gamma}^{(1)} \equiv U_{\lambda_V \frac{1}{2} \lambda_\gamma \frac{1}{2}}, \quad T_{\lambda_V \lambda_\gamma}^{(2)} \equiv T_{\lambda_V \frac{1}{2} \lambda_\gamma -\frac{1}{2}}, \quad U_{\lambda_V \lambda_\gamma}^{(2)} \equiv U_{\lambda_V \frac{1}{2} \lambda_\gamma -\frac{1}{2}}. \quad (2.3)$$

All other amplitudes can be obtained from the symmetry relations given by Eqs. (2.1 – 2.2). The HARs extracted in the present analysis are defined for  $n = 1, 2$  as  $t_{\lambda_V \lambda_\gamma}^{(n)} = \frac{T_{\lambda_V \lambda_\gamma}^{(n)}}{T_{00}^{(1)}}$ ,  $u_{\lambda_V \lambda_\gamma}^{(n)} = \frac{U_{\lambda_V \lambda_\gamma}^{(n)}}{U_{00}^{(1)}}$ .

### 3. Data Analysis

The data were accumulated with the HERMES spectrometer using the 27.6 GeV longitudinally polarized electron or positron beam of HERA, and gaseous hydrogen or deuterium targets. The HERMES forward spectrometer is described in Ref. [9]. The spectrometer permitted a precise measurement of charged-particle momenta with a resolution of 1.5%. A separation of leptons was achieved with an average efficiency of 98% and a hadron contamination below 1%.

The  $\omega$  and  $\rho^0$  mesons are produced and decay in the following exclusive reactions:  $e + p \rightarrow e + p + V$ ,  $\omega \rightarrow \pi^+ + \pi^- + \pi^0$ ,  $\pi^0 \rightarrow 2\gamma$  for  $V = \omega$  and  $\rho^0 \rightarrow \pi^+ + \pi^-$  when  $V = \rho^0$ . The following requirements were applied for event selection in  $\omega$ -meson production:

- i) Exactly two oppositely charged hadrons and one lepton with the same charge as the beam lepton are identified.
- ii) A  $\pi^0$  meson that is reconstructed from two calorimeter clusters is selected requiring the two-photon invariant mass to be in the interval  $0.11 \text{ GeV} < M(\gamma\gamma) < 0.16 \text{ GeV}$ .
- iii) The three-pion invariant mass is required to obey  $0.71 \text{ GeV} \leq M(\pi^+ \pi^- \pi^0) \leq 0.87 \text{ GeV}$ .
- iv) The scattered-lepton momentum lies above 3.5 GeV.
- v) Taking into account the spectrometer resolution, the missing energy  $\Delta E$  has to lie in the interval  $-1.0 \text{ GeV} < \Delta E < 0.8 \text{ GeV}$ . Here,  $\Delta E = \frac{M_X^2 - M_p^2}{2M_p}$ , with  $M_p$  being the proton mass and  $M_X^2 = (p + q - p_{\pi^+} - p_{\pi^-} - p_{\pi^0})^2$  the missing mass squared, where  $p$ ,  $q$ ,  $p_{\pi^+}$ ,  $p_{\pi^-}$ , and  $p_{\pi^0}$  are the four-momenta of target nucleon, virtual photon, and each of the three pions respectively.
- vi) The constraints  $Q^2 > 1.0 \text{ GeV}^2$ ,  $6.3 \text{ GeV} > W > 3 \text{ GeV}$ ,  $-t' < 0.2 \text{ GeV}^2$  are applied.

After application of all these constraints, the proton sample contains 2260 and the deuteron sample 1332 events of exclusively produced  $\omega$  mesons. These data samples are referred to in the following as data in the “entire kinematic region”. The distribution of missing energy  $\Delta E$ , shown in Fig. 1, exhibits a clearly visible exclusive peak. The shaded histogram represents semi-inclusive deep-inelastic scattering (SIDIS) background obtained from a PYTHIA Monte Carlo simulation that is normalized to the data in the region of  $2 \text{ GeV} < \Delta E < 20 \text{ GeV}$ . The simulation is used to determine the fraction of background under the exclusive peak. It amounts to about 20% for the entire kinematic region.

The only requirements changed for event selection in  $\rho^0$ -meson production were:

- ii) No calorimeter clusters were observed (no  $\pi^0$  is detected).
  - iii) The two-pion invariant mass is required to obey  $0.7 \text{ GeV} \leq M(\pi^+ \pi^-) \leq 1.0 \text{ GeV}$ .
  - vi) The constraint  $-t' < 0.4 \text{ GeV}^2$  is applied.
- The total number of reconstructed events with  $\rho^0$  mesons exclusively produced on the transversely polarized proton (transverse polarization  $P_T = 0.72 \pm 0.06$ ) was 8741.

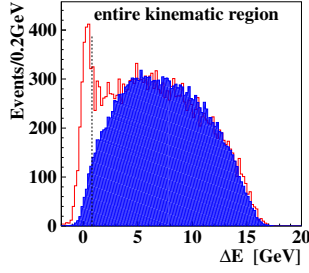


**Figure 1:** The  $\Delta E$  distribution of  $\omega$  mesons produced in the entire kinematic region. The vertical dashed line denotes the upper limit of the exclusive region.

#### 4. Results

In exclusive electroproduction, SDMEs are fitted as parameters of the experimental angular distribution of the final particles. The “unpolarized” SDMEs can be obtained from scattering of unpolarized initial particles while the “polarized” SDMEs can be extracted only from data collected with a longitudinally polarized beam. The results on SDMEs are obtained using an unbinned maximum likelihood method. All details of the fit procedure including the method of taking into account the background corrections are described in Ref. [5].

The SDMEs of the  $\omega$  and  $\rho^0$  mesons for the entire kinematic region are compared in Fig. 2. The SDMEs for  $\omega$  are extracted at  $\langle Q^2 \rangle = 2.42 \text{ GeV}^2$ ,  $\langle W \rangle = 4.8 \text{ GeV}$ ,  $\langle -t' \rangle = 0.080 \text{ GeV}^2$  while for  $\rho^0$  production  $\langle Q^2 \rangle = 1.95 \text{ GeV}^2$ ,  $\langle W \rangle = 4.8 \text{ GeV}$ , and  $\langle -t' \rangle = 0.13 \text{ GeV}^2$ . These SDMEs are divided into five classes corresponding to various helicity transitions  $\lambda_\gamma \rightarrow \lambda_V$ . The main terms in the expressions of class-A SDMEs correspond to the transitions from longitudinal virtual photons to longitudinal vector mesons,  $\gamma_L^* \rightarrow V_L$ , and from transverse virtual photons to transverse vector mesons,  $\gamma_T^* \rightarrow V_T$ . The dominant terms of class B correspond to the interference of these two transitions. The main terms of class-C, D, and E SDMEs are proportional to small amplitudes of  $\gamma_T^* \rightarrow V_L$ ,  $\gamma_L^* \rightarrow V_T$ , and  $\gamma_T^* \rightarrow V_{-T}$  transitions respectively.

The SDMEs for the proton and deuteron data are found to be consistent with one another within their combined total uncertainties. In Fig. 2, the uncertainties of the polarized SDMEs are larger than those of the unpolarized SDMEs because the mean polarization  $\langle |P_b| \rangle \approx 40\%$  and the polarized SDMEs are multiplied by the small factor  $|P_b| \sqrt{1 - \varepsilon} \approx 0.2$  in the equation for the angular distribution. Here,  $\varepsilon$  is the ratio of fluxes of the longitudinally and transversely polarized virtual photons. The linear combination of the class-A and class-B SDMEs, which are to be zero if S-Channel Helicity Conservation (SCHC) approximation is valid, are really zero within experimental uncertainties (see Ref. [5]). All SDMEs of classes C, D, E are to be zero in the SCHC approximation. The SDME  $r_0^5$  violates SCHC both for the  $\rho^0$  and  $\omega$  mesons since it is nonzero as is seen from Fig. 2.

As is also seen the SDMEs,  $r_{1-1}^1$  and  $\text{Im}\{r_{1-1}^2\}$  have opposite sign for  $\omega$  and  $\rho^0$  mesons. The explanation follows from the expressions of these SDMEs in terms of the amplitudes given in [7, 8]:  $|T_{11}|^2 > |U_{11}|^2$  for the  $\rho^0$  meson, while  $|U_{11}|^2 > |T_{11}|^2$  for the  $\omega$  meson. Moreover, the contribution of the UPE amplitude  $U_{11}$  dominates in the cross section of the  $\omega$ -meson production while its contribution for the  $\rho^0$ -meson electroproduction is small [8]. As the simplest consequence

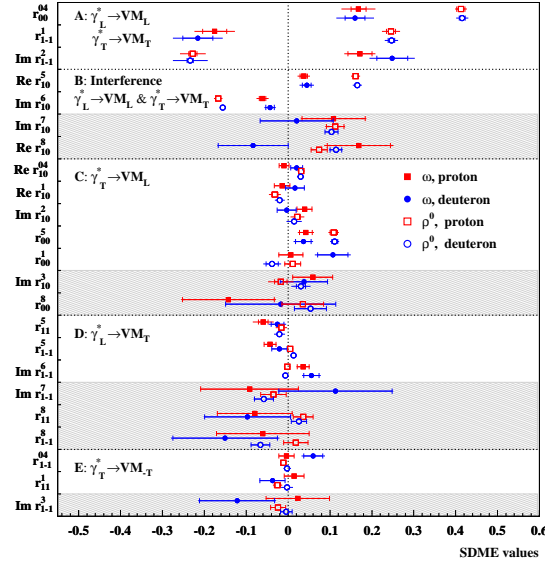


**Figure 2:** Comparison of 23 SDMEs for  $\omega$  and  $\rho^0$  [8] for the entire kinematic region. The inner error bars represent the statistical uncertainties, while the outer ones indicate the statistical and systematic uncertainties added in quadrature. Unpolarized (polarized) SDMEs are displayed in the unshaded (shaded) areas.

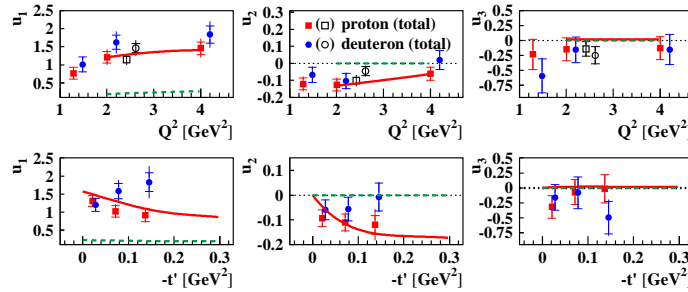


**Figure 3:** The  $Q^2$  and  $-t'$  dependences of  $u_1$ ,  $u_2$ , and  $u_3$ , where  $u_1 = 1 - r_{00}^{04} + 2r_{1-1}^{04} - 2r_{11}^1 - 2r_{1-1}^1$ ,  $u_2 = r_{11}^5 + r_{1-1}^5$ , and  $u_3 = r_{11}^8 + r_{1-1}^8$ . The open symbols represent the values over the entire kinematic region. Solid (dashed) curves are obtained in the GK model when the pion exchange is (not) taken into account. The error bars are the same as in Fig. 2.

of UPE dominance, the values of the SDME combinations  $u_1$ ,  $u_2$ , and  $u_3$  are unexpectedly large for the  $\omega$  meson as is seen from Fig. 3. These combinations are well described in the GK model [3], if the pion exchange is included in the calculation, as can be seen from a comparison of solid and dashed curves with the HERMES data.

The HARs obtained from the 25-parameter fit in the entire kinematic region ( $\langle W \rangle = 4.73$  GeV,  $\langle Q^2 \rangle = 1.93$  GeV<sup>2</sup>,  $\langle -t' \rangle = 0.132$  GeV<sup>2</sup>) are shown in Fig. 4. While the phase of  $u_{11}^{(1)}$  is fixed according to the results of Refs. [10, 11], its modulus is fit so that the two crosses represent the

results of fitting one free parameter. The value of  $\text{Im}[t_{11}^{(1)}]$  (open square) represents the result of Ref. [6]; its error bar shows the total uncertainty. The shadowed area corresponds to results that are also obtained in Ref. [6], while all other points are calculated for the first time. As is seen from Fig. 4, all HARs except  $t_{11}^{(1)}$ ,  $t_{01}^{(1)}$ , and  $u_{11}^{(1)}$ , are compatible with zero within their total uncertainties. The HAR  $t_{01}^{(1)}$  is responsible for SCHC violation, while  $u_{11}^{(1)}$  shows the role of UPE in  $\rho^0$  production.

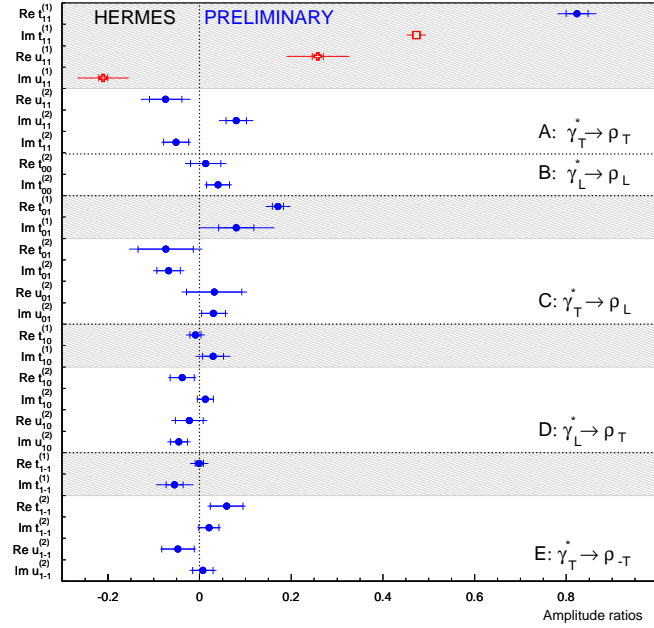


**Figure 4:** Helicity-amplitude ratios in the entire kinematic region. The inner error bars represent the statistical uncertainty, while the outer ones represent statistical and systematic uncertainties added in quadrature.

## References

- [1] M. Diehl, *Phys. Rep.* **388** (2003) 41.
- [2] J.C. Collins, L. Frankfurt, M.S. Strikman, *Phys. Rev.* **D56** (1997) 2982.
- [3] S. Goloskokov, P. Kroll, *Eur. Phys. J.* **A50** (2014) 146.
- [4] L. Morand et al. (CLAS Collaboration), *Eur. Phys. J.* **A24** (2005) 445.
- [5] A. Airapetian et al. (HERMES Collaboration), *Eur. Phys. J.* **C74** (2014) 3110.
- [6] A. Airapetian et al., (HERMES Collaboration), *Eur. Phys. J.* **C71** (2011) 1609.
- [7] K. Schilling, G. Wolf, *Nucl. Phys.* **B61** (1973) 381.
- [8] A. Airapetian et al. (HERMES Collaboration), *Eur. Phys. J.* **C62** (2009) 659.
- [9] Ackerstaff K et al. (HERMES Collaboration), *Nucl. Instr. and Meth.* **A417** (1998) 230.
- [10] A. Airapetian et al. (HERMES Collaboration), *Phys. Lett.* **B513** (2001) 301.
- [11] A. Airapetian et al. (HERMES Collaboration), *Eur. Phys. J.* **C29** (2003) 171.